UNIVERSITY *of* York

This is a repository copy of *Control of dynamic sp3-C stereochemistry*.

White Rose Research Online URL for this paper:
https://eprints.whiterose.ac.uk/198543/

Version: Published Version

Article:

McGonigal, Paul Ronald James orcid.org/0000-0002-8538-7579 and Bismillah, Aisha (2023) Control of dynamic sp3-C stereochemistry. Nature Chemistry. ISSN 1755-4349

https://doi.org/10.1038/s41557-023-01156-7

White Rose
university consortium
Universities of Leeds, Sheffield & York

eprints@whiterose.ac.uk
https://eprints.whiterose.ac.uk/

Article

Control of dynamic sp^3-C stereochemistry

Aisha N. Bismillah[1], Toby G. Johnson [1], Burhan A. Hussein[1], Andrew T. Turley[1], Promeet K. Saha [1], Ho Chi Wong[1], Juan A. Aguilar [1], Dmitry S. Yufit[1] & Paul R. McGonigal [1,2]✉

Stereogenic sp^3-hybridized carbon centres are fundamental building blocks of chiral molecules. Unlike dynamic stereogenic motifs, such as sp^3-nitrogen centres or atropisomeric biaryls, sp^3-carbon centres are usually fixed, requiring intermolecular reactions to undergo configurational changes. Here we report the internal enantiomerization of fluxional carbon cages and the consequences of their adaptive configurations for the transmission of stereochemical information. The sp^3-carbon stereochemistry of the rigid tricyclic cages is inverted through strain-assisted Cope rearrangements, emulating the low-barrier configurational dynamics typical for sp^3-nitrogen inversion or conformational isomerism. This dynamic enantiomerization can be stopped, restarted or slowed by external reagents, while the configuration of the cage is controlled by neighbouring, fixed stereogenic centres. As part of a phosphoramidite–olefin ligand, the fluxional cage acts as a conduit to transmit stereochemical information from the ligand while also transferring its dynamic properties to chiral-at-metal coordination environments, influencing catalysis, ion pairing and ligand exchange energetics.

The hugely varied three-dimensional (3D) structures—and therefore the hugely varied properties—of many organic molecules emerge from combining just a few types of atomic building blocks. For example, 19 of the 22 proteinogenic amino acids are formed solely from sp^2- or sp^3-hybridized carbon, nitrogen and oxygen atoms, capped by hydrogen substituents. Of this small array of elemental building blocks, it is tetrahedral sp^3-carbon[1–4] and sp^3-nitrogen[5–10] atoms that have the potential to form stereogenic centres, creating chiral structures.

Chirality also arises in organic molecules by virtue of motifs other than stereogenic atoms. However, although stereochemical inversion of some planar chiral motifs[11–13], helices[14–16] and stereogenic sp^3-nitrogen centres[7–10] can occur rapidly and reversibly through low-barrier conformational isomerism, sp^3-carbon centres cannot generally undergo spontaneous stereochemical changes. For example, the energy barrier to pyramidal inversion of methane is greater than its C–H bond dissociation energy[17–19]. Accordingly, unlike other stereogenic motifs[11–16], sp^3-carbon centres cannot generally adapt to surrounding chiral moieties and cannot be controllably switched by the application of external stimuli.

Instead, intermolecular reactions are usually necessary[20,21] to invert individual stereogenic carbon centres, proceeding through

mechanisms involving high-energy bond-breaking and bond-making steps[22] with pentavalent transition states[20] (for example, S_N2 reactions) or trigonal intermediates[21], such as carbocations, carbanions or radicals. Of course, it is this stability of sp^3-carbon's tetrahedral geometry that makes it essential to the chiral skeletal diversity of organic compounds. It allows for predictable synthesis of configurationally stable molecules. Yet, the stability also limits the extent to which the complex 3D connectivity of aliphatic structures can exhibit dynamic, adaptive stereochemistry[23].

There have been impressive, but rare, examples of small covalent systems[24–28] capable of sp^3-carbon enantiomerization by low-barrier intramolecular processes. However, they do so without external control of their rate or direction to a single stereoisomer. Only multicomponent interlocked molecules, in which a ring shuttles along a prochiral axle[29,30], have been amenable to external control. There have been no compact and controllable dynamic sp^3-carbon building blocks. Therefore, it has not been possible to investigate the transmission of stereochemical information through such systems[7,9,10].

In this Article we report a series of chiral fluxional carbon cages[26–29] that exhibit responsive sp^3-carbon-centred stereochemistry, adapting to and transmitting surrounding stereochemical information.

[1]Department of Chemistry, Durham University, Durham, UK. [2]Department of Chemistry, University of York, York, UK. ✉e-mail: paul.mcgonigal@york.ac.uk
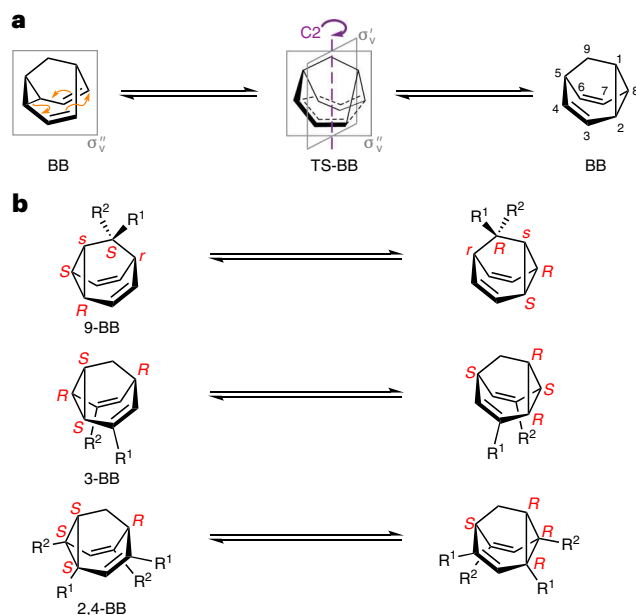
Fig. 1 | Multiple dynamic sp^3-carbon centres. a,b, Fluxional sp^3-carbon stereochemistry arises in BBs when the structures interchanged by their Cope rearrangements (**a**) are desymmetrized with any of the three substitution patterns shown in **b**. Cahn–Ingold–Prelog priorities are chosen to be $R^1 > C > R^2$ for the assignment of absolute configuration. When assigning a descriptor to position 9 of 9-BB, the cyclopropyl bridgehead C1 has precedence over the divinyl bridgehead C5 (Supplementary Fig. 1). 3-BB and 2,4-BB each have four chirotopic (R/S) centres, whereas the 9-BB pattern gives rise to five stereogenic centres, of which three are chirotopic and two are achirotopic (r/s).

By applying density functional theory (DFT) calculations and solution- and solid-state NMR spectroscopy, in combination with X-ray crystallography, we establish the extent to which their dynamic Cope rearrangements[31,32] are controlled by neighbouring, fixed stereogenic centres. We have found that a substantial energetic bias of more than 10 kJ mol⁻¹ can be exercised over the stereochemical equilibria by a single fixed stereocentre. The rearrangements proceed rapidly at rates more commonly associated with low-barrier conformational changes of aliphatic systems (for example, a cyclohexane ring-flip energy barrier of ~43 kJ mol⁻¹) rather than a configurational change. We show that these rapid constitutional dynamics can be halted by covalent modification of the cage through a [2 + 2 + 2] cycloaddition reaction, then subsequently restarted after a cycloreversion. The rearrangement rate is also attenuated upon coordination of the fluxional cage to Pd(II) or Ru(II) as part of a phosphoramidite–olefin ligand. By its inclusion in the simple ligand design, the fluxional cage transmits stereochemical information to the metal ion—either through the covalent ligand backbone or by ion pairing with a chiral counterion. This property is exploited in enantioselective catalysis of an allylic substitution reaction, as well as in creating chiral-at-metal stereogenic centres that adopt the configurational dynamics of the cage.

Results

The Cope rearrangement of barbaralane (BB) is an example (Fig. 1a) of a narcissistic[25,33] automerization—it gives rise to a degenerate structure through a transition state (TS-BB) bearing an internal mirror plane (σ'_v) that is not present in the minimum energy structure. We noted that by desymmetrizing BB (Fig. 1b) using either a 9-BB, 3-BB or 2,4-BB substitution pattern, the mirror plane present at the energy minimum (σ''_v) is lost, while the mirror plane formed in the transition state (σ'_v) is retained. As a result, the Cope rearrangement inverts simultaneously some, or all, of the four or five stereogenic centres present in the structure. Given that the rearrangement of BB is known to proceed with a

remarkably low free energy of activation, $\Delta G^{\ddagger}$, of 32.3 kJ mol⁻¹ (Supplementary Table 7)[34–38], chiral 9-BB, 3-BB or 2,4-BB derivatives should undergo rapid enantiomerization.

Diastereomeric adaptation

We targeted 9-BB **1** (Fig. 2) as a convenient example of the 9-BB substitution pattern that bears a hydroxyl group for synthetic elaboration. The Cope rearrangement involving positions 2–8 of **1** (Fig. 2a) causes enantiomerization of the whole cage and formally inverts the stereochemistry of position 9 by effectively 'swapping' the cyclopropyl and alkene substituents connected to the stereocentre. Compound **1** was synthesized (Supplementary Scheme 1) by a three-step route from ethynylmagnesium bromide and tropylium tetrafluoroborate, using a gold-catalysed enyne cycloisomerization[39,40] to form the BB backbone. When labelling **1** and subsequent compounds, a single stereochemical descriptor is included to indicate the configuration at position 9 of the BB (Fig. 2a), for example, (R)-**1** and (S)-**1**, omitting the additional stereochemical labels of positions 1, 2, 5 and 8 for simplicity (Fig. 1). Treatment of **1** with Mosher's acid chloride (Fig. 2a) produces a set of Mosher's esters **2** in which the configurationally fixed stereocentre is introduced at a distance of three covalent bonds from the dynamic BB unit. An additional descriptor for the configuration of the Mosher's ester group is included in the labels for **2**. Derivatization with (S)-Mosher's acid gives a dynamic mixture of two diastereomers, (R,S)-**2** and (S,S)-**2**, whereas (R)-Mosher's acid gives (Fig. 2a) the antipodal mixture, (S,R)-**2** and (R,R)-**2**. Solutions of the two antipodal dynamic mixtures give opposite circular dichroism spectra (Fig. 3a), as would be expected.

DFT modelling using the ωB97X-D functional[41], 6-311++G(d,p) basis set[42,43] and a CS₂ polarizable continuum solvent model using the integral equation formalism variant[44] was employed to compare (Supplementary Table 7) the stereoisomerization energetics of BB, **1** and **2**. Using these parameters, the automerization of BB is predicted to proceed with a calculated activation free energy, $\Delta G^{\ddagger}_{calc}$, of 38.5 kJ mol⁻¹, which is ~6 kJ mol⁻¹ higher than the experimentally measured[35] activation free energy, $\Delta G^{\ddagger}_{exp}$, of 32.3 kJ mol⁻¹, in keeping with previous DFT investigations[36,37]. DFT methods systematically overestimate the energy barrier to Cope rearrangement of BBs, but nevertheless allow useful comparisons of trends in activation energies and are known to predict accurately the relative energy minima of isomers[36,37]. The computationally predicted $\Delta G^{\ddagger}_{calc}$ values for **1** (38.0 kJ mol⁻¹) and **2** (35.5 kJ mol⁻¹) are very similar to BB, indicating that the hydroxyl or ester group substitutions at position 9 do not appreciably change the rapid kinetics.

The absence of the σ''_v mirror plane in **1** is evident (Fig. 3b) in its solution-state ¹H NMR spectrum—H3 and H7 are magnetically inequivalent, for example. However, the rapid enantiomerization induces a σ'_v mirror plane to the time-averaged structure of **1**, so only six distinct methine resonances are observed overall. The additional, fixed stereocentre of **2** breaks this σ'_v symmetry. Consequently, nine distinct signals corresponding to the BB methine groups are observed (Fig. 3b).

An energy difference, ΔG_{calc}, of 4.5 kJ mol⁻¹ is computed (Supplementary Table 7) for the rearrangement of **2**. The influence of the (S)-Mosher's ester group moulds the configuration of the cage unit, which preferentially adopts its S form, biasing the equilibrium towards (S,S)-**2**. Consistent with this prediction, a single crystal (Fig. 2a) obtained from the dynamic (S)-Mosher's ester mixture was found to contain (S,S)-**2** as a frozen[34], single stereoisomer. An equal and opposite outcome is observed from the (R)-Mosher's ester mixture, giving the enantiomeric (R,R)-**2** solid-state structure.

To establish the nature of the dynamic solution-state mixtures, we compared (Fig. 3c) the solid-state ¹³C{¹H} NMR spectrum of enantiopure (R,R)-**2** crystals to a spectrum obtained using a sample of the (S,S)-**2** crystals dissolved in 5:1 CS₂–CD₂Cl₂, generating a dynamic mixture of (R,S)-**2** and (S,S)-**2**. Cooling the solution to 159 K causes the BB ¹³C{¹H} NMR resonances to enter the slow exchange regime.
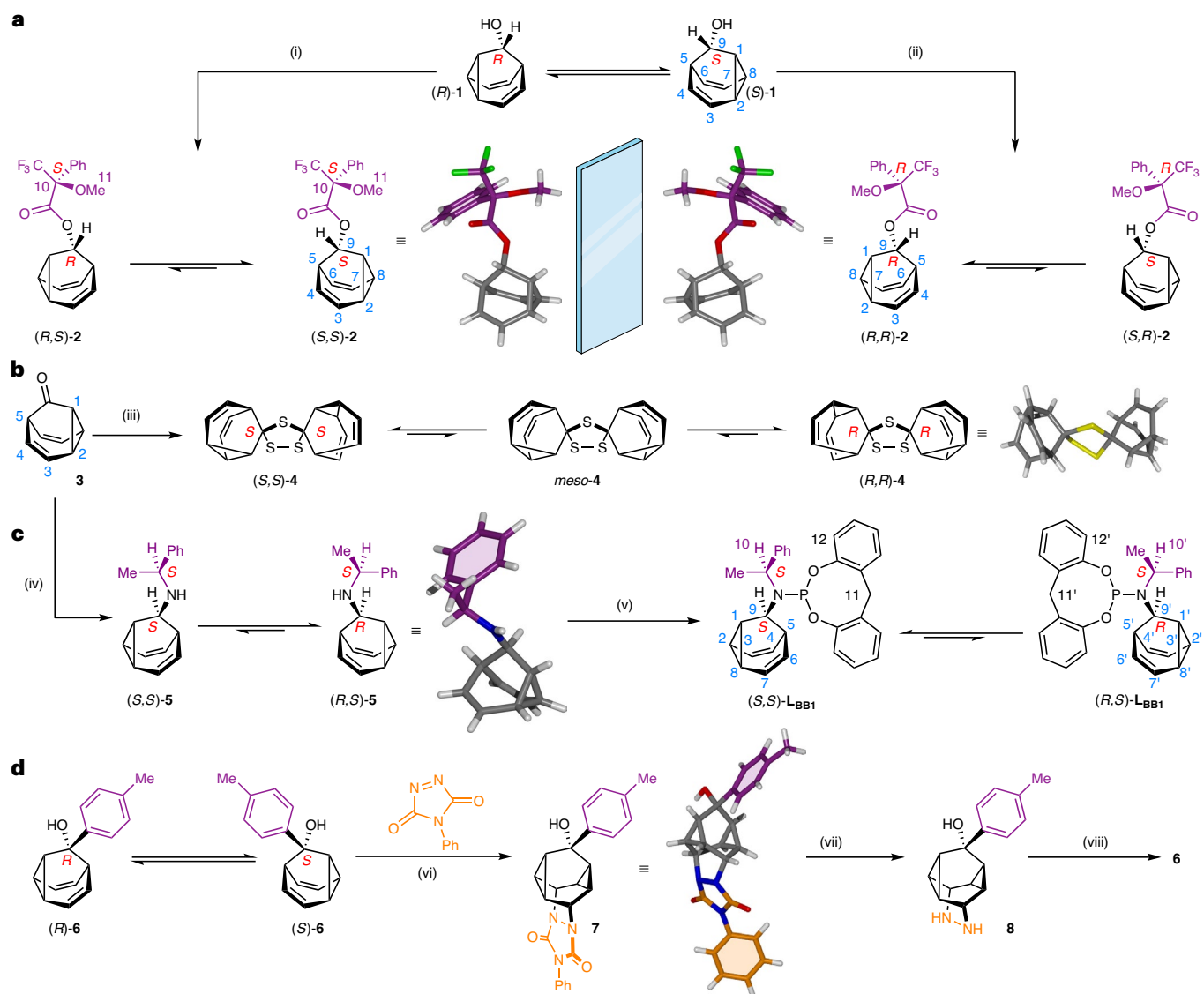
Fig. 2 | Diastereomeric adaptation and manipulation of chiral BBs. a,b, The dynamic sp^3-C stereochemical equilibrium of the BB cage is degenerate in **1** but becomes biased towards one stereoisomer upon attaching a chiral auxiliary (**a**) or by dimerization through a spirocyclic bridge (**b**). **c,** The position of the stereochemical equilibrium changes (and inverts) upon modifying the structure of a chiral auxiliary, remote from the BB unit. **d,** Further control of the sp^3-C stereochemistry is exerted by a cycloaddition reaction, which freezes and symmetrizes the structure, before subsequent cycloreversion re-establishes the dynamic stereochemical equilibrium. Reagents and conditions: (i) 1. (S)-MTPA, (COCl)$_2$, hexanes, DMF, room temperature (r.t.) to −20 °C, 16 h. 2. **1**, DMAP, Et$_3$N, CHCl$_3$, r.t., 5 d, 58%. (ii) 1. (R)-MTPA, (COCl)$_2$, hexanes, DMF, r.t. to −20 °C, 16 h. 2.

1, DMAP, Et$_3$N, CHCl$_3$, r.t., 3 d, 79%. (iii) **3**, Lawesson's reagent, PhMe, 110 °C, 18 h, 13%. (iv) 1. **3**, (S)-1-phenylethylamine, AcOH, MeOH, r.t., 30 min. 2. NaBH$_3$CN, 100 °C, 16 h, 89%. (v) **5**, PCl$_3$, Et$_3$N, CH$_2$Cl$_2$, 0 °C, 3 h. 2. 2,2'-methylenediphenol, CH$_2$Cl$_2$, 0 °C to r.t., 16 h, 44%. (vi) **6**, PTAD, CH$_2$Cl$_2$, 50 °C, 24 h, 85%. (vii) **7**, NaOH, ^{i}PrOH, 85 °C, 24 h, taken on crude. (viii) CuCl$_2$, HCl$_{(aq)}$, 0 °C, 4 h, 48% from **7**. X-ray structures are shown in stick representation. Compound **4** crystallizes in a centrosymmetric space group, that is, (S,S)-**4** and (R,R)-**4** are both present, but only (R,R)-**4** is shown for clarity. Diffraction data for crystals of (R,S)-**5** allow only assignment of relative stereochemistry. MTPA, α-methoxy-α-trifluoromethylphenylacetic acid; DMF, N,N-dimethylformamide; DMAP, 4-(dimethylamino)pyridine; PTAD, phenyl-1,2,4-triazoline-3,5-dione.

As 159 K is only ~20 K below the observed coalescence temperature (Supplementary Fig. 66) for this low-barrier process, some resonances exhibit exchange broadening. At this low temperature, the decrease of available thermal energy causes the Boltzmann distribution to shift (Fig. 3d) further towards the lowest-energy isomer[34]. The solid-state chemical shifts of the BB sp^3-carbons 1, 2, 5, 8 and 9 are assigned (Fig. 3b) by comparison to the calculated chemical shifts of (R,R)-**2**. The resonances of the solution sample match up well with those of (R,R)-**2** in the solid state, allowing us to assign the resolved solution-state diastereomer as (S,S)-**2**. The solution-state analysis is thus consistent with the diastereomeric preference predicted by DFT and observed in the solid state. The 9-BB cage undergoes dynamic diastereomeric

adaptation under the influence of the configurationally fixed Mosher's ester group.

The dynamic stereochemical equilibrium can also be biased in the absence of a fixed stereogenic element. Dimerization of two 9-BB-type cages through a spirocyclic linkage breaks the degeneracy of the equilibrium. By treating (Fig. 2b) barbaralone **3** with Lawesson's reagent, we isolated trithiolane **4**, which undergoes dynamic rearrangements between an achiral isomer, meso-**4**, and a pair of enantiomers, (S,S)-**4** and (R,R)-**4**. A small ΔG_{calc} of 0.7 kJ mol^{-1} is predicted (Supplementary Table 7) to favour the pair of enantiomers over the meso form in the solution state. Single crystals grown from a solution of **4** contain a racemic mixture of the two chiral stereoisomers.
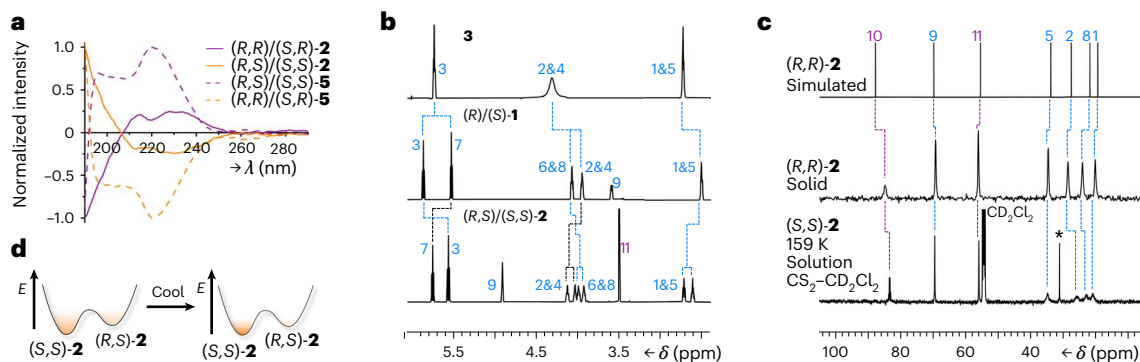
Fig. 3 | Spectroscopic evidence of sp^3-carbon adaptation to covalently tethered chiral auxiliaries. a, Normalized circular dichroism spectra of **2** (115 μM in MeCN) and **5** (210 μM in MeCN) confirm that antipodal equilibrium mixtures give equal and opposite absorbances. **b**, A comparison of partial solution ^{1}H NMR spectra (CDCl$_3$, 298 K) shows the reduced symmetry of the chiral 9-BB motif: top, **3** (700 MHz); middle, (*R*)/(*S*)-**1** (600 MHz); bottom, (*R,S*)/(*S,S*)-**2** (600 MHz). Resonances are labelled according to the numbering in Fig. 2. **c**, Comparison of partial ^{13}C{^{1}H} NMR spectra: top, solid-state chemical shifts calculated from the X-ray crystal structure of (*R,R*)-**2** in CASTEP v17.2[65]

using the Perdew–Burke–Ernzerhof functional[66] and on-the-fly generated pseudopotentials; middle, (*R,R*)-**2** as a powder at ambient temperature (105 MHz); bottom, (*S,S*)-**2** as a solution in 5:1 CS$_2$–CD$_2$Cl$_2$ at low temperature (125 MHz, 159 K). The asterisk indicates the resonance of residual acetone. **d**, The Boltzmann distribution of isomers shifts towards a single stereoisomer at low temperatures; for example, a free energy difference of -5 kJ mol^{-1} would give an -90:10 equilibrium mixture at room temperature, but >98:2 at 159 K, so NMR data would be expected to show a single, major species, as is apparent when comparing the three spectra in **c**.

Further chemical modification to the substituent at position 9 can substantially influence, and even invert, the cage's equilibrium distribution. The chiral phosphoramidite–olefin[45–47] ligand **L$_{BB1}$** was synthesized (Fig. 2c) by first subjecting **3** to reductive amination with (*S*)-1-phenylethylamine to afford a mixture of (*S,S*)-**5** and (*R,S*)-**5**. Sequential treatment of the amine with PCl$_3$ then 2,2′-methylenediphenol affords **L$_{BB1}$**. The 2,2′-methylenediphenol functionality was selected as it lacks fixed stereochemistry but has been shown to adopt dynamically chiral conformations as part of phosphoramidite ligands[45]. Comparing **L$_{BB1}$** to **5** reveals that the differing size and shape of the substituent at position 9 drives the dynamic stereochemical equilibria of the fluxional cage towards opposite configurations. The solution-phase equilibrium of the secondary amine is weighted (Supplementary Table 7) towards the (*R,S*)-**5** diastereomer by a ΔG_{calc} of 3.8 kJ mol^{-1}, matching the structure observed by X-ray analysis (Fig. 2c) of a single crystal. By contrast, the (*S,S*)-**L$_{BB1}$** diastereomer of the phosphoramidite is favoured with a ΔG_{calc} of 20.2 kJ mol^{-1}. The large magnitude of ΔG_{calc} for **L$_{BB1}$** highlights that the configurational dynamics of the 9-BB motif (Fig. 1) correlate with notable changes in its 3D shape[34] and, therefore, its energy. At the same time, the opposing stereochemistry of cages **5** and **L$_{BB1}$** demonstrates that the malleable sp^3-carbon configuration adapts to changes in the nearby steric environment.

Manipulating rates and transfer of stereochemistry

To exert further control over the fluxional enantiomerization, we sought to exploit the reactivity of the BBs' skipped diene units. The fluxional rearrangements can be stopped entirely by engaging the alkene units in covalent bonding, whereas coordination of the π electrons to a transition-metal ion[38] modulates the rearrangement rate instead.

An enantiomerizing mixture of 9-(*p*-tolyl)barbaralol **6** engages (Fig. 2d) in a [2 + 2 + 2] cycloaddition reaction with phenyl-1,2,4-triazoline-3,5-dione[48], giving rise to **7**. This reaction halts the rearrangement while also symmetrizing the structure by forming a second cyclopropyl group. Subsequently, the fluxional cage can be regenerated (Fig. 2d) in a two-step transformation through diazinane **8** (Supplementary Fig. 62), which undergoes cycloreversion with loss of N$_2$ upon oxidation with CuCl$_2$. Alternatively, coordination of Pd(II) (Fig. 4) or Ru(II) (Fig. 5) to **L$_{BB1}$** causes a reduction in the rate of the Cope rearrangement, as discussed below.

L$_{BB1}$ and PdCl$_2$ form (Fig. 4a) a chiral-at-metal[49,50] complex, **L$_{BB1}$**PdCl$_2$, linking the sp^3-carbon configurational inversion to the *A*/*C* isomerism[51] of the distorted trigonal bipyramidal (*TBPY*-5-12) coordination environment (Supplementary Fig. 2). Both possible stereoisomers, arising from coordination of (*S,S*)-**L$_{BB1}$** or (*R,S*)-**L$_{BB1}$** through their phosphorus centre and an alkene, are observed (Fig. 4a) in the X-ray crystal structure of the **L$_{BB1}$**PdCl$_2$ complex. The alkene coordination is also evident (Fig. 4b) in the solution state by ^{1}H NMR spectroscopy. For comparison, a monodentate **L$_{BB1}$**AuCl complex (Fig. 4a) was prepared, which shows only small changes in the ^{1}H NMR chemical shifts of its alkene signals H3 and H7 relative to the free ligand (Fig. 4b). The room-temperature spectrum of **L$_{BB1}$**PdCl$_2$, on the other hand, reveals a large change in the chemical shift of H7, consistent with coordination of Pd(II) to the alkene on the same face as the phosphoramidite group.

At 240 K, the ^{1}H NMR spectrum reveals (Fig. 4b) the two **L$_{BB1}$**PdCl$_2$ isomers in slow exchange. Two sets of signals are observed in a 3:4 ratio, corresponding to a small free energy difference, ΔG_{exp}, of 0.5 kJ mol^{-1} between the two isomers. Consistent with this observation, DFT calculations predict (Supplementary Table 7) a small ΔG_{calc} of 1.8 kJ mol^{-1} in favour of (*C,R,S*)-**L$_{BB1}$**PdCl$_2$.

Further NMR and DFT analyses elucidate the mechanism by which the **L$_{BB1}$**PdCl$_2$ complex isomerizes. Depending on the placement and nature of substituents around the Cope substrate, metal coordination can either stabilize a charged, intermediate species as part of a stepwise associative rearrangement mechanism, or it can increase the rate of a concerted rearrangement pathway by stabilizing the transition state[52]. Consequently, Pd(II) salts and other cationic metal ions are known to accelerate Cope rearrangements[53,54]. Remarkably, coordination of the Pd(II) to one face of the fluxional cage in **L$_{BB1}$**PdCl$_2$ has the opposite effect, slowing down the Cope rearrangement. Unlike **2**, for example, whose ^{1}H NMR resonances (499 MHz) enter the slow exchange regime below 160 K (Supplementary Fig. 64), the slower rearrangement of **L$_{BB1}$**PdCl$_2$ is resolved by ^{1}H NMR spectroscopy at the higher temperature of 240 K. Using 2D ^{1}H–^{1}H exchange spectroscopy (EXSY) at 240 K (Fig. 4c), we measured a rate of exchange, k, of 6.48 s^{-1}, indicating a $\Delta G^{\ddagger}_{exp}$ of 54.6 kJ mol^{-1} for **L$_{BB1}$**PdCl$_2$ (Fig. 4d). The DFT-calculated transition-state structure (Fig. 4e) shows pairs of equidistant C–C bonds, as would be expected for a coordination-coupled Cope (cc-Cope) rearrangement (Fig. 4a) in which the Pd(II) remains bound to the cage through a concerted rearrangement step. The DFT-predicted
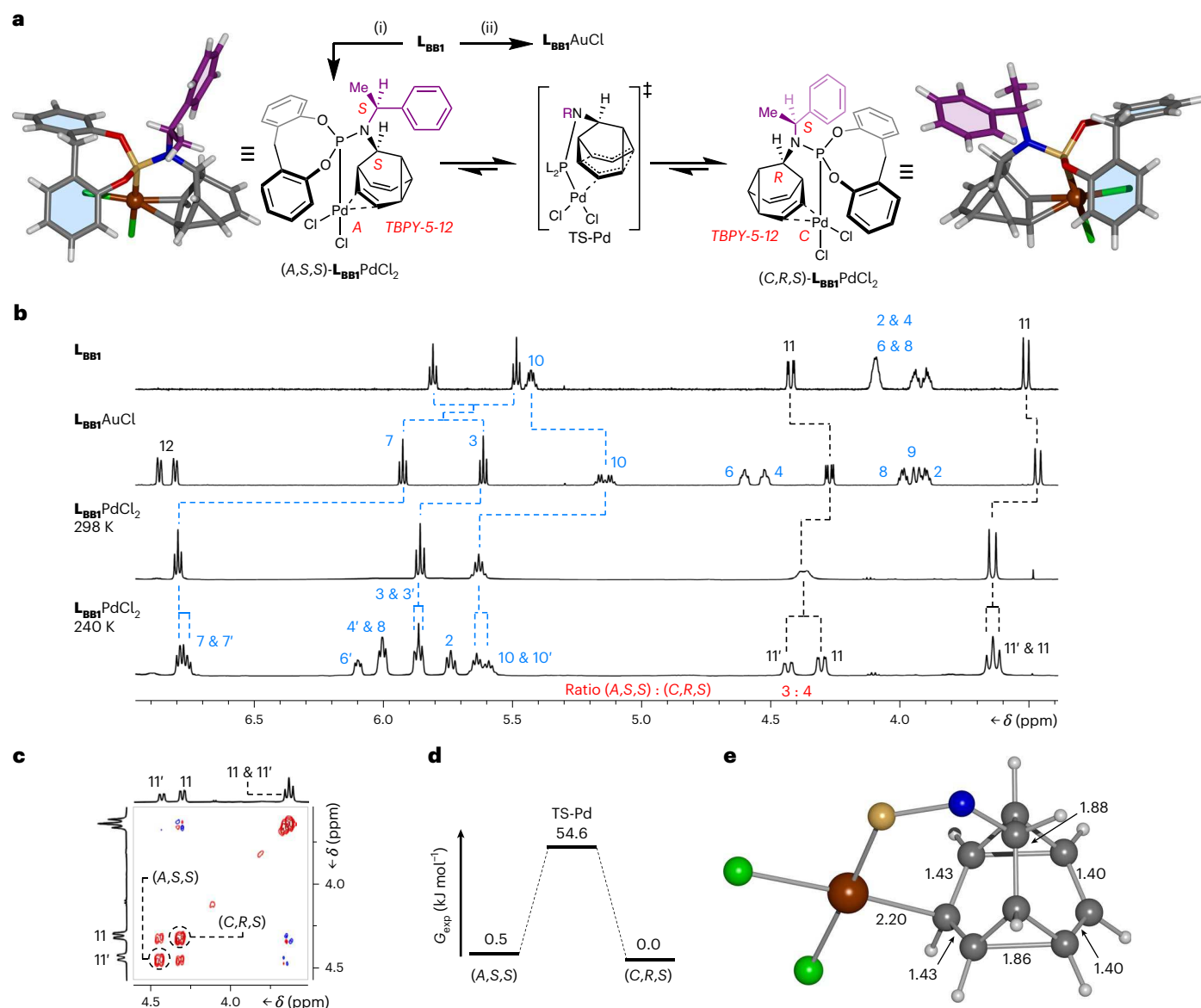
Fig. 4 | Transfer of dynamic sp^3-carbon stereochemistry in Au(I) and Pd(II) complexes. a, Bidentate coordination of $\mathbf{L_{BB1}}$ to $PdCl_2$ leads to cc-Cope rearrangement in which the Pd 'walks' along the side of the BB cage, modulating the rearrangement rate. For comparison, monodentate ligand coordination is observed with AuCl. Reagents and conditions: (i) $\mathbf{L_{BB1}}$, $PdCl_2(NCMe)_2$, $CDCl_3$, r.t., 15 min, 98%. (ii) $\mathbf{L_{BB1}}$, $Me_2S \cdot AuCl$, $CDCl_3$, r.t., 10 min, 93%. X-ray crystal structures are shown in stick representation, with a ball for metal ions. Solvent molecules are omitted for clarity. Two structurally similar conformers of each $\mathbf{L_{BB1}}PdCl_2$ stereoisomer are present in the unit cell, but only one of each is shown for clarity. **b**, Partial ^1H NMR ($CDCl_3$) spectra: top, $\mathbf{L_{BB1}}$ (599 MHz, 298 K); second row, $\mathbf{L_{BB1}}AuCl$ (599 MHz, 298 K); third row, $\mathbf{L_{BB1}}PdCl_2$ (499 MHz, 298 K); bottom,

$\mathbf{L_{BB1}}PdCl_2$ (499 MHz, 240 K). Resonances are labelled according to the numbering for $\mathbf{L_{BB1}}$ in Fig. 2. The spectrum at 240 K shows the two $\mathbf{L_{BB1}}PdCl_2$ complexes in slow exchange in a ratio of 3:4. **c**, A partial ^1H-^1H EXSY NMR spectrum (499 MHz, $CDCl_3$, 240 K, mixing time $\tau_m = 200$ ms) showing exchange peaks (red) between resonances of the minor ($H_{11'}$) and major (H_{11}) diastereomers as well as COSY peaks (blue) of geminal proton pairs. **d**, Free energy diagram for the cc-Cope rearrangement. **e**, Ball-and-stick representation of the DFT-calculated (ωB97X-D/6-311++G(d,p)/SDD/CS_2)[67] geometry of $\mathbf{L_{BB1}}PdCl_2$, showing the BB cage at the transition state, TS-Pd. A truncated structure omitting phosphorus and nitrogen substituents is shown for clarity with selected bond lengths given in ångstroms.

$\Delta G^{\ddagger}_{calc}$ of 60.6 kJ mol⁻¹ for this cc-Cope mechanism matches well with the $\Delta G^{\ddagger}_{exp}$ of 54.6 kJ mol⁻¹.

These data indicate that the metal ion 'walks' along one side of the BB cage as the Cope rearrangement proceeds, moving back and forth in sync with the pericyclic reaction[52]. Consequently, the BB not only transmits the stereochemical information from the fixed sp^3-carbon stereocentre through its dynamic sp^3-carbon framework, biasing the chiral-at-metal configuration, but it also imparts a novel mechanism of intramolecular configurational change at a pentavalent stereocentre, which differs from the established pseudorotation and turnstile mechanisms[55].

The dynamic sp^3-carbon stereochemistry of $\mathbf{L_{BB1}}$ can also be linked to an intermolecular ligand exchange process. The cyclopentadienyl (Cp) half-sandwich Ru(II) complex[56] $\mathbf{L_{BB1}}RuCp(NCMe) \cdot PF_6$ (Fig. 5) has a stereogenic, distorted square pyramidal Ru(II) centre (Supplementary Fig. 91) coordinated to a labile MeCN ligand. While cc-Cope rearrangements interconvert the SPY-5-21 and SPY-5-23 configurational isomers[51] (Fig. 5a), MeCN dissociation forms the distorted tetrahedral (T-4) chiral-at-metal species $\mathbf{L_{BB1}}RuCp \cdot PF_6$, which mediates A/C stereochemical inversion.

Ru(II) coordination slows the Cope rearrangement sufficiently for a single stereoisomer to be resolved as a metastable species
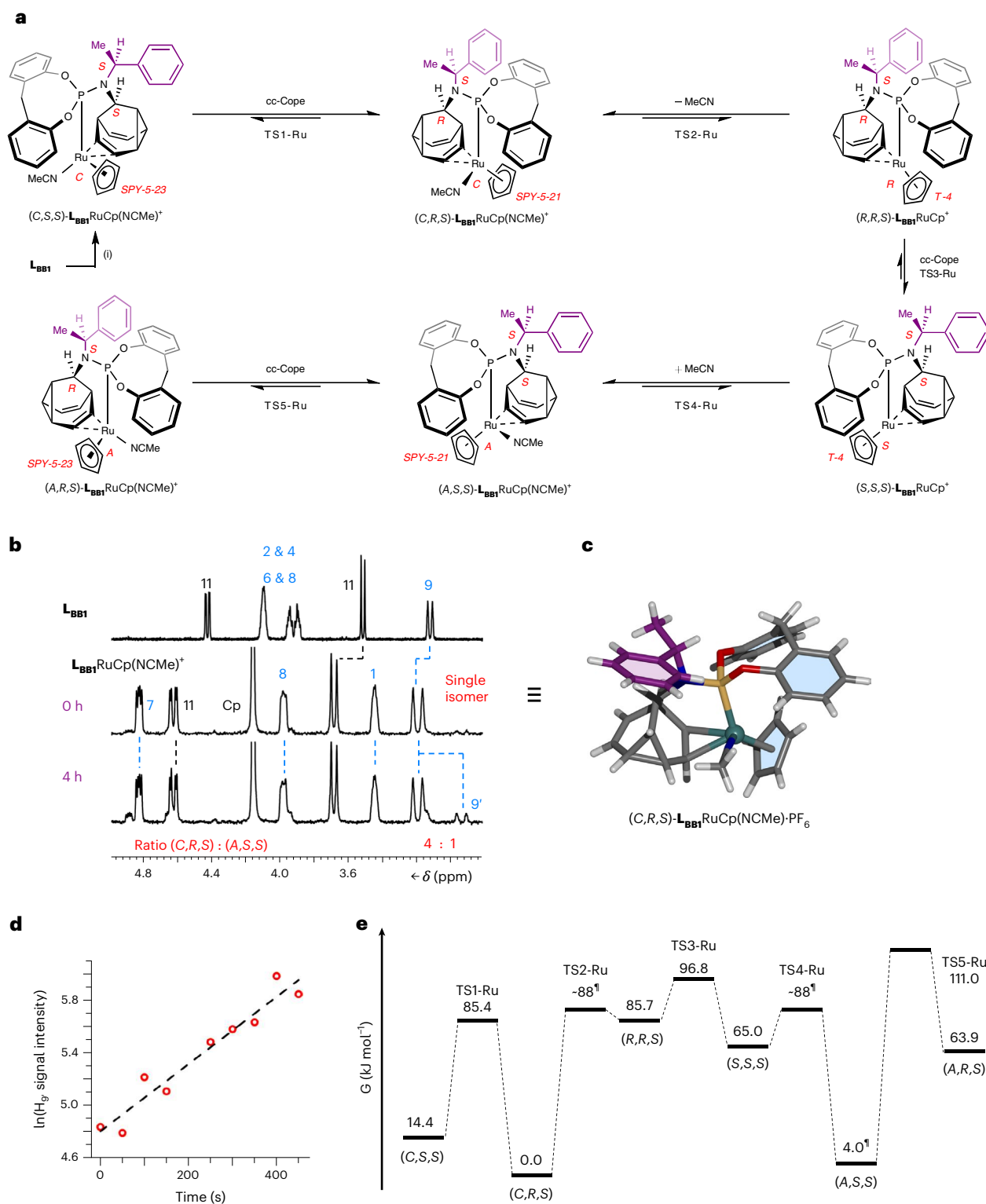
Fig. 5 | Transfer of dynamic sp^3-carbon stereochemistry in chiral-at-Ru(II) complexes. a, Four diastereomeric square pyramidal complexes are linked by cc-Cope rearrangements and exchange of an MeCN ligand, which proceeds through two intermediate tetrahedral complexes. A non-coordinated PF_6^- counterion is omitted from the structural formula of each complex for clarity. Reagents and conditions: (i) L_{BB1}, CpRu(NCMe)$_3$·PF$_6$, CDCl$_3$, r.t., 5 min, 69%. **b**, Comparison of the partial ^{1}H NMR (CDCl$_3$, 298 K) spectra: top, L_{BB1} (599 MHz); middle, a sample of L_{BB1}RuCp(NCMe)·PF$_6$ analysed immediately after dissolving a crystalline sample (400 MHz); bottom, the same sample after allowing it to equilibrate for 4 h (400 MHz), revealing that an initially observed single isomer reaches a 4:1 equilibrium mixture. Resonances are labelled according to the

numbering for L_{BB1} in Fig. 2. **c**, (C,R,S)-L_{BB1}RuCp(NCMe)·PF$_6$ is identified in the solid-state X-ray crystal structure, which is shown in stick representation with a ball for the Ru(II) ion. Solvent molecules and the PF$_6^-$ counterion are omitted for clarity. **d**, Integration of the ^{1}H NMR (400 MHz, CDCl$_3$, 298 K) resonance corresponding to H9′ of (A,S,S)-L_{BB1}RuCp(NCMe)·PF$_6$ upon dissolving a crystalline sample of (C,R,S)-L_{BB1}RuCp(NCMe)·PF$_6$ reveals a first-order increase in concentration with $k_{obs} = 2.56 \times 10^{-3}$ s^{-1}. **e**, A potential energy surface for isomerization for the cc-Cope processes. Values of ΔG_{calc} and $\Delta G_{calc}^{\ddagger}$ (ωB97X-D/6-311++G(d,p)/SDD/CS$_2$)[67] are given except where ¶ indicates experimentally measured (**b**,**d**) equilibrium (ΔG_{exp}) and ligand exchange ($\Delta G_{exp}^{\ddagger}$) energies (in units of kJ mol^{-1}).
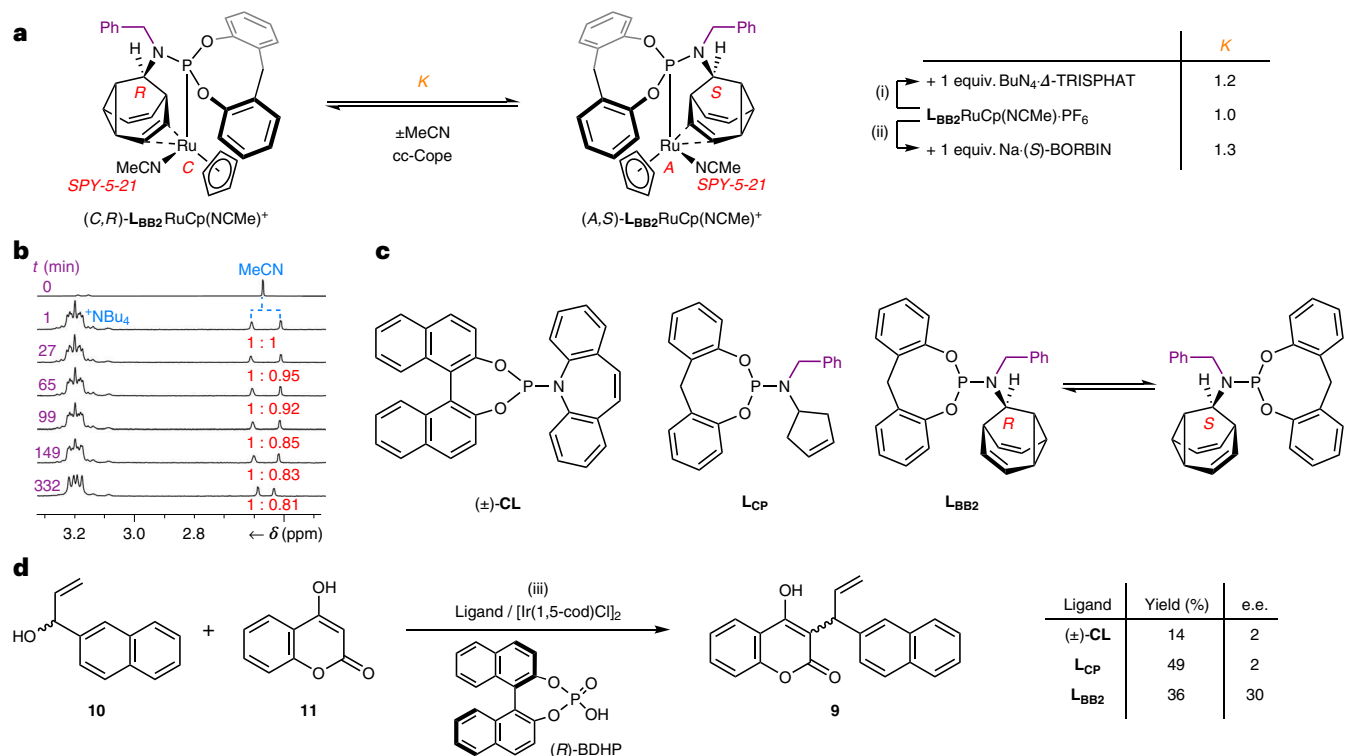
Fig. 6 | Chiral counterion-directed sp3-carbon and chiral-at-metal stereochemistry applied to enantioselective catalysis. a, The enantiomerization of $L_{BB2}RuCp(NCMe)^+$ is degenerate in the presence of an achiral counterion. In the presence of chiral anions, the ion-pair interactions break the degeneracy and bias the equilibrium towards one stereoisomer of the BB–metal complex, that is, $K \neq 1$. Note: only the two lowest-energy stereoisomers are shown for clarity. Reagents and conditions: (i) $L_{BB2}RuCp(NCMe)\cdot PF_6$, $BuN_4\cdot\Delta$-TRISPHAT, CDCl$_3$, r.t. (ii) $L_{BB2}RuCp(NCMe)\cdot PF_6$, Na·(S)-BORBIN, CDCl$_3$, r.t. **b**, Comparison of the partial ^{1}H NMR spectra (400 MHz, CDCl$_3$, 298 K) of $L_{BB2}RuCp(NCMe)\cdot PF_6$ before (top row) and after (other rows) the addition of 1 equiv. of $BuN_4\cdot\Delta$-TRISPHAT. Integration of the MeCN resonances shows that the initially racemic $L_{BB2}RuCp(NCMe)^+$ ion gradually becomes enriched in one stereoisomer ($K = 1.2$). **c,d**, The stereoinduction (**c**) arising from three phosphoramidite ligands was compared in an iridium-catalysed allylic substitution (**d**). We hypothesize that the chiral anion formed in situ biases the stereochemical equilibrium of the cationic $L_{BB2}Ir$ π-allyl intermediate, leading to its improved performance relative to the control ligands lacking dynamic sp^3-C stereochemistry. Reagents and conditions: (iii) 1. [Ir(1,5-cod)Cl$_2$] (4 mol%), ligand (16 mol%), THF, 30 min, r.t. 2. (R)-BDHP (10 mol%), r.t., 24 h. Δ-TRISPHAT, Δ-tris(tetrachloro-1,2-benzenediolato)phosphate(V); (S)-BORBIN, bis[(S)-1,1'-bis-2-naphtholato]borate; 1,5-cod, 1,5-cyclooctadiene; (R)-BDHP, (R)-1,1'-binaphthyl-2,2'-diyl hydrogen phosphate.

under ambient conditions (Fig. 5b). Upon dissolving single crystals of $L_{BB1}RuCp(NCMe)\cdot PF_6$, obtained by slow evaporation, the ^{1}H NMR spectrum shows the presence of a single complex (Fig. 5b) with resonances distinct from non-coordinated L_{BB1}. After allowing the sample to fully equilibrate at room temperature for four hours, a new set of peaks is observed (Fig. 5b) at a ratio of 4:1 in favour of the initially observed isomer, equivalent to a ΔG_{exp} of 4.0 kJ mol^{-1}. X-ray analysis (Fig. 5c) of the crystalline sample reveals the identity of the energetically favoured isomer to be (C,R,S)-$L_{BB1}RuCp(NCMe)\cdot PF_6$.

We measured the isomerization rate of (C,R,S)-$L_{BB1}RuCp(NCMe)\cdot PF_6$ by monitoring (Fig. 5d) the first-order growth in intensity of the resonance at 3.1 ppm corresponding to the H9' signal of (A,S,S)-$L_{BB1}RuCp(NCMe)\cdot PF_6$—the isomer calculated (Fig. 5e) to be the next most stable stereoisomer. The k_{obs} of 2.56×10^{-3} s^{-1} at 298 K allows us to determine a $\Delta G_{exp}^{\ddagger}$ of 87.8 kJ mol^{-1}. Comparison of this value to (1) maxima of the computed potential energy surface (Fig. 5e), (2) a CD$_3$CN exchange experiment (Supplementary Fig. 70) and (3) literature measurements of MeCN dissociation from Cp half-sandwich Ru(II) complexes[55] suggests that the cc-Cope and MeCN exchange processes occur at similar rates. To achieve the (C,R,S)-to-(A,S,S) isomerization observed by NMR, the complex must undergo both ligand exchange and cc-Cope steps (Fig. 5e). Overall, the energetic bias towards (C,R,S)-$L_{BB1}RuCp(NCMe)\cdot PF_6$ and observation of its stepwise stereomutation to (A,S,S)-$L_{BB1}RuCp(NCMe)\cdot PF_6$ illustrate that the fluxional sp^3-carbon cage mediates the transfer of stereochemical information with high fidelity from the single, fixed benzylamino stereocentre through its rigid, tricyclic structure.

Dynamic stereocontrol by ion pairing

Having observed transmission of stereochemical information within the covalent frameworks of the L_{BB1} complexes, we investigated the influence of chiral counterions[57] on the degenerate enantiomerization (Fig. 6a) of the cationic $L_{BB2}RuCp(NCMe)^+$ complex, which lacks a fixed stereocentre in its ligand structure. The complex was synthesized (Supplementary Scheme 3) as its hexafluorophosphate salt, $L_{BB2}RuCp(NCMe)\cdot PF_6$, in a manner analogous to its permanently chiral homologue $L_{BB1}RuCp(NCMe)\cdot PF_6$ (Fig. 5). X-ray analysis of single crystals confirmed (Supplementary Fig. 94) the expected structure of $L_{BB2}RuCp(NCMe)\cdot PF_6$ and revealed the presence (Supplementary Fig. 95) of both the (C,R)- and (A,S)-isomers in the crystal unit cell.

In the absence of chiral anions, a single ^{1}H NMR signal is observed for the coordinated MeCN ligand of $L_{BB2}RuCp(NCMe)\cdot PF_6$ in CDCl$_3$ solution (Fig. 6b). However, the addition of one molar equivalent of a chiral shift reagent, Bu$_4$N·Δ-TRISPHAT[58] (Fig. 6b) or Na·(S)-BORBIN[59] (Supplementary Fig. 71), splits the signal in two. Rapid and reversible counterion exchange in the presence of Bu$_4$N·Δ-TRISPHAT establishes an equilibrium mixture that includes diastereomeric ion pairs, for example, (C,R)-$L_{BB2}RuCp(NCMe)\cdot\Delta$-TRISPHAT and (A,S)-$L_{BB2}RuCp(NCMe)\cdot\Delta$-TRISPHAT, which give distinct NMR resonances. Therefore, by tracking the relative intensities of these resonances over time (Fig. 6b and Supplementary Fig. 72) we can monitor changes in sample composition as the chiral anion biases the $L_{BB2}RuCp(NCMe)^+$ complex towards one stereoisomer. Under these conditions, the Δ-TRISPHAT sample evolves from a 1:1 mixture of stereoisomers to a

1:0.81 mixture over several hours, corresponding to an equilibrium constant, K, of 1.2, and $\Delta G_{exp} \approx 0.5$ kJ mol^{-1}. The timeframe of the sample's evolution is consistent with the slow kinetics of isomerization measured (Fig. 5) for $\mathbf{L_{BB1}}$RuCp(NCMe)·PF$_6$, suggesting that the stereomutation is again proceeding by cc-Cope and MeCN ligand exchange. The (S)-BORBIN sample reaches (Supplementary Fig. 72) a K of 1.3 over a similar time period. Overall, these experiments establish a means of noncovalent control of the BB stereochemistry. In principle, K could be further increased by removal or omission of any competing achiral anions (such as PF$_6^-$) from the reaction mixture and optimization of solvent and concentration.

Based on these results, we hypothesized that this counterion-directed stereochemistry of cationic $\mathbf{L_{BB2}}$ complexes could be exploited in enantioselective ion-pair catalysis[60]. Unusually, the fixed stereochemistry of the chiral anion would be passed to the catalytically active, fluxional metal complex to transiently generate an enantioenriched ligand framework in situ. To probe this concept, we screened $\mathbf{L_{BB2}}$ and two control ligands (Fig. 6c) in the enantioselective synthesis of **9** (Fig. 6d) through iridium-catalysed allylic substitution of alcohol **10** by hydroxycoumarin **11**[61]. We used chiral phosphoric acid (R)-BDHP, which we expected to protonate **10** and induce formation of the iridium-stabilized allylic cation intermediate while simultaneously generating an equivalent of a chiral phosphate anion. The optimized literature conditions[61] for this allylic substitution employ an achiral Lewis acid (Yb(OTf)$_3$) rather than a Brønsted acid to generate the allylic cation, in conjunction with enantiopure Carreira's[46] phosphoramidite–olefin ligand, **CL**, to impart enantioselectivity. Pleasingly, replacing these reagents with (R)-BDHP and racemic (±)-**CL** leads to the formation of **9**, albeit in just 14% isolated yield. Importantly, however, there is essentially no enantioinduction under the influence of (±)-**CL**. The product is obtained with a negligible enantiomeric excess (e.e.) of just 2%. It appears that the chiral phosphoric acid alone does little to override the stereochemical preference (or overall lack of it) arising from the racemic ligand. Using achiral phosphoramidite–olefin ligand $\mathbf{L_{CP}}$ leads to a similar outcome. $\mathbf{L_{CP}}$ bears many of the same structural features of $\mathbf{L_{BB2}}$, but with an achiral cyclopentene unit in place of the dynamically chiral 9-BB substructure. Compound **9** is produced in 49% yield and just 2% e.e. using $\mathbf{L_{CP}}$. Conversely, our fluxionally chiral ligand, $\mathbf{L_{BB2}}$, delivers an improved e.e. Using $\mathbf{L_{BB2}}$, we isolated **9** in 36% yield and 30% e.e. Contrasting this result with the outcome of the reactions using $\mathbf{L_{CP}}$ and (±)-**CL** supports the idea that the chiral phosphate counterion biases the covalent $\mathbf{L_{BB2}}$ ligand stereochemistry of the cationic intermediate complex (Supplementary Scheme 5), which in turn improves the enantioinduction in the key bond-forming step. Although the resulting e.e. is moderate for this particular set of reaction conditions, it suggests that the use of fluxional sp^3-carbon units may enhance the design of ligand frameworks for ion-pair catalysis[60] and other forms of enantioselective synthesis.

Conclusions
Cope rearrangements of chiral 9-BB cages simultaneously invert every stereogenic sp^3-carbon centre of their structures. These configurational rearrangements occur rapidly and reversibly, achieving the uncommon property of dynamic sp^3-carbon stereochemistry—one that has remained surprisingly rare since Le Bel[1] and van't Hoff[2] first identified tetrahedral carbon as a source of molecular chirality in 1874. Both the rate of sp^3-carbon inversion and the equilibrium distribution of isomers are sensitive to changes in the 9-BB structure. On the one hand, the dynamics of the rearrangement processes are controlled through manipulation of covalent bonding or metal coordination of the 9-BB olefin groups, providing convenient functional handles. On the other hand, the cage adapts its configuration to minimize steric interactions with nearby fixed stereogenic elements and, in so doing, is able to transmit the stereochemical information across its rigid, tricyclic backbone. When interfaced with transition-metal complexes, the dynamic cage

conveys a stereochemical preference to the chiral-at-metal[49,50] centre. Controllable and adaptable sp^3-carbon stereochemistry of this kind can be exploited in enantioselective synthesis[7,9,10,30,45,62,63] and chiral functional materials[64].

Online content
Any methods, additional references, Nature Portfolio reporting summaries, source data, extended data, supplementary information, acknowledgements, peer review information; details of author contributions and competing interests; and statements of data and code availability are available at https://doi.org/10.1038/s41557-023-01156-7.

References
1. Le Bel, J. A. Sur les relations qui existent entre les formules atomiques des corps organiques, et le pouvoir rotatoire de leurs dissolutions. *Bull. Soc. Chim. Fr.* **22**, 337–347 (1874).
2. van't Hoff, J. H. Sur les formules de structure dans l'espace. *Arch. Néerl.* **9**, 445–454 (1874).
3. Eliel, E. L. & Wilen, S. H. *Stereochemistry of Organic Compounds* (Wiley, 1994).
4. Quasdorf, K. W. & Overman, L. E. Catalytic enantioselective synthesis of quaternary carbon stereocentres. *Nature* **516**, 181–191 (2014).
5. Brois, S. J. Aziridines. XII. Isolation of a stable nitrogen pyramid. *J. Am. Chem. Soc.* **90**, 508–509 (1968).
6. Kizirian, J. C. Chiral tertiary diamines in asymmetric synthesis. *Chem. Rev.* **108**, 140–205 (2008).
7. Sibi, M. P., Zhang, R. & Manyem, S. A new class of modular chiral ligands with fluxional groups. *J. Am. Chem. Soc.* **125**, 9306–9307 (2003).
8. Rowley, J. H., Yau, S. C., Kariuki, B. M., Kennedy, A. R. & Tomkinson, N. C. O. Readily accessible chiral at nitrogen cage structures. *Org. Biomol. Chem.* **11**, 2198–2205 (2013).
9. Adachi, S., Takeda, N. & Sibi, M. P. Evaluation of achiral templates with fluxional Brønsted basic substituents in enantioselective conjugate additions. *Org. Lett.* **16**, 6440–6443 (2014).
10. Dean, C. et al. Readily accessible sp^3-rich cyclic hydrazine frameworks exploiting nitrogen fluxionality. *Chem. Sci.* **11**, 1636–1642 (2020).
11. Fa, S., Egami, K., Adachi, K., Kato, K. & Ogoshi, T. Sequential chiral induction and regulator-assisted chiral memory of pillar[5]arenes. *Angew. Chem. Int. Ed.* **59**, 20353–20356 (2020).
12. Liang, H. et al. Acid/base-tunable unimolecular chirality switching of a pillar[5]azacrown *pseudo*[1]catenane. *J. Am. Chem. Soc.* **142**, 19772–19778 (2020).
13. Xiao, C. et al. Redox-triggered chirality switching and guest-capture/release with a pillar[6]arene-based molecular universal joint. *Angew. Chem. Int. Ed.* **59**, 8094–8098 (2020).
14. Akine, S., Sairenji, S., Taniguchi, T. & Nabeshima, T. Stepwise helicity inversions by multisequential metal exchange. *J. Am. Chem. Soc.* **135**, 12948–12951 (2013).
15. Chen, X. et al. A helicate-based three-state molecular switch. *Angew. Chem. Int. Ed.* **57**, 11817–11820 (2018).
16. Katoono, R., Sakamoto, K. & Suzuki, T. Dual dynamic chirality generated in the assembly of three achiral rods through the three-fold twisting of a macrocycle. *Chem. Commun.* **55**, 5503–5506 (2019).
17. Hoffmann, R., Alder, R. W. & Wilcox, C. F. Planar tetracoordinate carbon. *J. Am. Chem. Soc.* **92**, 4992–4993 (1970).
18. Gordon, M. S. & Schmidt, M. W. Does methane invert through square planar? *J. Am. Chem. Soc.* **115**, 7486–7492 (1993).
19. Rasmussen, D. R. & Radom, L. Planar-tetracoordinate carbon in a neutral saturated hydrocarbon: theoretical design and characterization. *Angew. Chem. Int. Ed.* **38**, 2876–2878 (1999).
20. Walden, P. Ueber die gegenseitige Umwandlung optischer Antipoden. *Ber. Dtsch. Chem. Ges.* **29**, 133–138 (1896).

21. Kancharla, P. K., Kato, T. & Crich, D. Probing the influence of protecting groups on the anomeric equilibrium in sialic acid glycosides with the persistent radical effect. *J. Am. Chem. Soc.* **136**, 5472–5480 (2014).

22. Sugiyama, S. et al. A novel dynamic kinetic resolution accompanied by intramolecular transesterification: asymmetric synthesis of a 4-hydroxymethyl-2-oxazolidinone from serinol derivatives. *Tetrahedron* **59**, 3417–3425 (2003).

23. Wolf, C. *Dynamic Stereochemistry of Chiral Compounds* (RSC, 2007).

24. Kim, B. et al. Stereodynamic quinone-hydroquinone molecules that enantiomerize at sp^3-carbon via redox-interconversion. *J. Am. Chem. Soc.* **139**, 15239–15244 (2017).

25. Gillick-Healy, M. W. et al. Two independent orthogonal stereomutations at a single asymmetric center: a narcissistic couple. *Chem. A Eur. J.* **23**, 2332–2339 (2017).

26. He, M. & Bode, J. W. Racemization as a stereochemical measure of dynamics and robustness in shape-shifting organic molecules. *Proc. Natl. Acad. Sci. USA* **108**, 14752–14756 (2011).

27. Yahiaoui, O., Patel, H. D., Chinner, K. S., Paŝteka, L. F. & Fallon, T. Stereomutation of substituted bullvalenes. *Org. Lett.* **23**, 1157–1162 (2021).

28. Sanchez, A. & Maimone, T. J. Taming shapeshifting anions: total synthesis of ocellatusone C. *J. Am. Chem. Soc.* **144**, 7594–7599 (2022).

29. Alvarez-Pérez, M., Goldup, S. M., Leigh, D. A. & Slawin, A. M. Z. A chemically-driven molecular information ratchet. *J. Am. Chem. Soc.* **130**, 1836–1838 (2008).

30. Dommaschk, M., Echavarren, J., Leigh, D. A., Marcos, V. & Singleton, T. A. Dynamic control of chiral space through local symmetry breaking in a rotaxane organocatalyst. *Angew. Chem. Int. Ed.* **58**, 14955–14958 (2019).

31. Cope, A. C. & Hardy, E. M. The introduction of substituted vinyl groups. V. A rearrangement involving the migration of an allyl group in a three-carbon system. *J. Am. Chem. Soc.* **62**, 441–444 (1940).

32. Bismillah, A. N., Chapin, B. M., Hussein, B. A. & McGonigal, P. R. Shapeshifting molecules: the story so far and the shape of things to come. *Chem. Sci.* **11**, 324–332 (2020).

33. Salem, L. et al. Narcissistic reactions. *J. Am. Chem. Soc.* **92**, 4472–4474 (1970).

34. Bismillah, A. N. et al. Shape-selective crystallisation of fluxional carbon cages. *Chem. Sci.* **9**, 8631–8636 (2018).

35. Günther, H., Runsink, J., Schmickler, H. & Schmitt, P. Applications of ^{13}C NMR spectroscopy. 26. Activation parameters for the degenerate Cope rearrangement of barbaralane and 3,7-disubstituted barbaralanes. *J. Org. Chem.* **50**, 289–293 (1985).

36. Ma, Y. Y. et al. Probing the fluxional bonding nature of rapid Cope rearrangements in bullvalene $C_{10}H_{10}$ and its analogs C_8H_8, C_9H_{10} and C_8BH_9. *Sci. Rep.* **9**, 17074 (2019).

37. Karton, A. Can density functional theory 'Cope' with highly fluxional shapeshifting molecules? *Chem. Phys.* **540**, 111013 (2021).

38. Aumann, R. & Runge, M. Organische Synthesen mit übergangsmetall-Komplexen, 57. 4,5-Homotropilidene durch intramolekulare Cyclopropanierung von (cycloheptatrie-nylmethyl)carbenchrom-oder-Wolfram-Komplexen. *Chem. Ber.* **125**, 259–264 (1992).

39. McGonigal, P. R. et al. Gold for the generation and control of fluxional barbaralyl cations. *Angew. Chem. Int. Ed.* **51**, 13093–13096 (2012).

40. Ferrer, S. & Echavarren, A. M. Synthesis of barbaralones and bullvalenes made easy by gold catalysis. *Angew. Chem. Int. Ed.* **55**, 11178–11182 (2016).

41. Chai, J.-D. & Head-Gordon, M. Long-range corrected hybrid density functionals with damped atom-atom dispersion corrections. *Phys. Chem. Chem. Phys.* **10**, 6615–6620 (2008).

42. Krishnan, R., Binkley, J. S., Seeger, R. & Pople, J. A. Self-consistent molecular orbital methods. XX. A basis set for correlated wave functions. *J. Chem. Phys.* **72**, 650–654 (1980).

43. Clark, T., Chandrasekhar, J., Spitznagel, G. W. & Schleyer, P. V. R. Efficient diffuse function-augmented basis sets for anion calculations. III. The 3-21+G basis set for first-row elements, Li–F. *J. Comput. Chem.* **4**, 294–301 (1983).

44. Miertuŝ, S. & Tomasi, J. Approximate evaluations of the electrostatic free energy and internal energy changes in solution processes. *Chem. Phys.* **65**, 239–245 (1982).

45. Wakabayashi, K., Aikawa, K., Kawauchi, S. & Mikami, K. Catalyst self-adaptation in conjugate addition to nitroalkenes and nitroacrylates: instant chirality control in diphenylmethane-based phosphoramidite ligands. *J. Am. Chem. Soc.* **130**, 5012–5013 (2008).

46. Rössler, S. L., Petrone, D. A. & Carreira, E. M. Iridium-catalyzed asymmetric synthesis of functionally rich molecules enabled by (phosphoramidite, olefin) ligands. *Acc. Chem. Res.* **52**, 2657–2672 (2019).

47. Teichert, J. F. & Feringa, B. L. Phosphoramidites: privileged ligands in asymmetric catalysis. *Angew. Chem. Int. Ed.* **49**, 2486–2528 (2010).

48. De Bruycker, K. et al. Triazolinediones as highly enabling synthetic tools. *Chem. Rev.* **116**, 3919–3974 (2016).

49. Bauer, E. B. Chiral-at-metal complexes and their catalytic applications in organic synthesis. *Chem. Soc. Rev.* **41**, 3153–3167 (2012).

50. Zhou, Z. et al. Non-C_2-symmetric chiral-at-ruthenium catalyst for highly efficient enantioselective intramolecular $C(sp^3)$-H amidation. *J. Am. Chem. Soc.* **141**, 19048–19057 (2019).

51. Connelly, N. G. et al. (eds) *Nomenclature of Inorganic Chemistry: IUPAC Recommendations 2005* (RSC, 2005).

52. Siebert, M. R. & Tantillo, D. J. Transition-state complexation in palladium-promoted [3,3] sigmatropic shifts. *J. Am. Chem. Soc.* **129**, 8686–8687 (2007).

53. Jiao, H. & von Ragué Schleyer, P. Elimination of the barrier to Cope rearrangement in semibullvalene by Li^+ complexation. *Angew. Chem. Int. Ed. Engl.* **32**, 1760–1763 (1993).

54. Tantillo, D. J. Speeding up sigmatropic shifts—to halve or to hold. *Acc. Chem. Res.* **49**, 741–749 (2016).

55. Couzijn, E. P. A., Slootweg, J. C., Ehlers, A. W. & Lammertsma, K. Stereomutation of pentavalent compounds: validating the Berry pseudorotation, redressing Ugi's turnstile rotation, and revealing the two- and three-arm turnstiles. *J. Am. Chem. Soc.* **132**, 18127–18140 (2010).

56. Luginbühl, W. et al. Structure and reactivity of ruthenium half-sandwich compounds: crystal and molecular structure and acetonitrile exchange kinetics and mechanism of $Ru(\eta^6\text{-}C_6H_6)$$(CH_3CN)_3^{2+}$ and $Ru(\eta^5\text{-}C_5H_5)(CH_3CN)^{3+}$. *Inorg. Chem.* **30**, 2350–2355 (1991).

57. Corra, S. et al. Chemical on/off switching of mechanically planar chirality and chiral anion recognition in a [2]rotaxane molecular shuttle. *J. Am. Chem. Soc.* **141**, 9129–9133 (2019).

58. Lacour, J., Ginglinger, C., Favarger, F. & Torche-Haldimann, S. Application of TRISPHAT anion as NMR chiral shift reagent. *Chem. Commun.* **1997**, 2285–2286 (1997).

59. Raskatov, J. A., Brown, J. M. & Thompson, A. L. Chiral selection in the formation of borates from racemic binaphthols and related diols. *CrystEngComm* **13**, 2923–2929 (2011).

60. Fanourakis, A., Williams, B. D., Paterson, K. J. & Phipps, R. J. Enantioselective intermolecular C–H amination directed by a chiral cation. *J. Am. Chem. Soc.* **143**, 10070–10076 (2021).

61. Xu, R. et al. Direct enantioselective allylic substitution of 4-hydroxycoumarin derivatives with branched allylic alcohols via iridium catalysis. *Chem. Commun.* **56**, 8404–8407 (2020).

62. Wang, J. & Feringa, B. L. Dynamic control of chiral space. *Science* **331**, 1429–1432 (2011).

63. Heard, A. W. & Goldup, S. M. Synthesis of a mechanically planar chiral rotaxane ligand for enantioselective catalysis. *Chem* **6**, 994–1006 (2020).

64. Morrow, S. M., Bissette, A. J. & Fletcher, S. P. Transmission of chirality through space and across length scales. *Nat. Nanotechnol.* **12**, 410–419 (2017).

65. Clark, S. J. et al. First principles methods using CASTEP. *Z. Kristallogr.* **220**, 567–570 (2005).

66. Perdew, J. P., Burke, K. & Ernzerhof, M. Generalized gradient approximation made simple. *Phys. Rev. Lett.* **77**, 3865–3868 (1996).

67. Andrae, D., Häußermann, U., Dolg, M., Stoll, H. & Preuß, H. Energy-adjusted ab initio pseudopotentials for the second and third row transition elements. *Theor. Chim. Acta* **77**, 123–141 (1990).

Publisher's note Springer Nature remains neutral with regard to jurisdictional claims in published maps and institutional affiliations.

Data availability

Crystallographic data for the structures reported in this Article have been deposited at the Cambridge Crystallographic Data Centre, under deposition numbers CCDC 2068012 (**1**), 2068013 (**4**), 2068014 ((*R*,*S*)-**5**), 2068015 ((*S*,*S*)-**2**), 2068016 ((*R*,*R*)-**2**), 2068017 (**7**), 2068018 (**L$_{BB1}$**PdCl$_2$), 2068019 (**S2**), 2068020 ((*C*,*R*,*S*)-**L$_{BB1}$**RuCp(NCMe)·PF$_6$) and 2173984 (**L$_{BB2}$**RuCp(NCMe)·PF$_6$). Copies of the data can be obtained free of charge via https://www.ccdc.cam.ac.uk/structures/. All other data supporting the findings of this study are available within the paper and its Supplementary Information.

Author contributions

A.N.B. synthesized **3** and **6**, carried out variable-temperature NMR spectroscopy, performed chiral anion experiments and enantioselective catalysis, and prepared the Supplementary Information. T.G.J. synthesized **2**, **4** and **5** and performed CD spectroscopy. B.A.H. and A.T.T. optimized the trapping and release of **6** by cycloaddition. A.N.B., P.K.S., A.T.T. and H.C.W. performed the preliminary experiments. J.A.A. assisted with NMR measurements. D.S.Y. solved X-ray crystal structures. A.N.B. and P.R.M. synthesized the ligands and metal complexes. P.R.M. conceived and directed the research, carried out DFT calculations and wrote the manuscript. All authors analysed the data and revised the manuscript.

Competing interests

The authors declare no competing interests.

Additional information

Supplementary information The online version contains supplementary material available at https://doi.org/10.1038/s41557-023-01156-7.

Correspondence and requests for materials should be addressed to Paul R. McGonigal.

Peer review information *Nature Chemistry* thanks the anonymous reviewer(s) for their contribution to the peer review of this work.

Reprints and permissions information is available at www.nature.com/reprints.